International Journal of Engineering and Technology Innovation, vol. 15, no. 3, 2025, pp. 254-275

Predicting Punching Shear Strength of RC Interior Flat Slabs Using an Attention-Based Transformer and Differential Evolution

Kamaran Kakel Hamd*

Department of Geomatics, College of Engineering, Salahaddin University, Erbil, Iraq

Received 24 December 2024; received in revised form 16 March 2025; accepted 20 March 2025

DOI: https://doi.org/10.46604/ijeti.2024.14661

Abstract

Punching shear strength (PSS) prediction in reinforced concrete (RC) interior flat slabs remains challenging for conventional empirical methods. Thus, this study proposes a hybrid attention-based transformer model optimized via differential evolution to address this limitation. The methodology combines multi-head attention mechanisms to capture nonlinear interactions among critical parameters (support dimensions, slab thickness, concrete strength, rate of steel bars, and steel yield strength). The model is trained and tested using 417 experimental results of flat slabs and processes eight input features encompassing geometric properties. The experimental results show superior accuracy, achieving a mean squared error (MSE) of 0.00017, a root mean squared error (RMSE) of 0.0113, and an R-squared of 0.998. The proposed model is benchmarked with well-known machine learning (ML) models and achieves a superior performance. These results emphasize the model's potential as a scalable and precise tool for predicting PSS in RC flat slabs.

Keywords: punching shear strength prediction, reinforced concrete, deep learning, differential evolution

1. Introduction

Punching shear strength (PSS) refers to the capacity of a slab to resist localized failure due to concentrated loading, typically around columns [1]. In the case of reinforced concrete (RC) interior flat slabs, punching shear occurs when the slab fails in a brittle manner around the support, like a column, due to excessive shear stress. This failure results in the slab "punching" down around the column perimeter. While the one-way shear occurs in beams or one-way slabs, where shear forces act along a single plane, causing diagonal tension cracks governed by longitudinal reinforcement and sectional geometry [2-3].

The PSS may be affected by several factors, viz. (a) column size and shape, as larger column areas reduce shear stress and increase shear resistance; (b) slab thickness, as thicker slabs provide more resistance to punching shear; (c) concrete compressive strength, where higher concrete strength enhances the punching shear capacity; (d) reinforcement ratio, where the amount and placement of reinforcement influence how well the slab resists shear stresses; (e) critical perimeter, defined as the perimeter around the column where punching shear is calculated; and (f) the type of loading, since punching shear is highly sensitive to the magnitude and distribution of loads [4].

RC flat slabs are extensively utilized in construction due to their structural efficiency and aesthetic flexibility. However, these slabs are vulnerable to the failure of punching shear, which is attributed to their limited shear-resisting area, especially around slab-column connections, as shown in Fig. 1. Such failures carry a significant risk of progressive structural collapse

* Corresponding author. E-mail address: kamaran.hamad@su.edu.krd

[5]. The PSS at these connections is a crucial factor in load-bearing capacity, whereas the slab's shallow depth often hinders the practical use of shear-resisting stirrups. Under high loads, sudden load reductions and cone-shaped failures around the column perimeter can occur without warning. To mitigate this weakness, the incorporation of steel fibers into concrete matrices to enhance punching shear resistance has been investigated. Steel fibers enhance concrete's ability to bridge cracks, control crack propagation, and improve its overall shear strength, toughness, and post-failure performance [6].

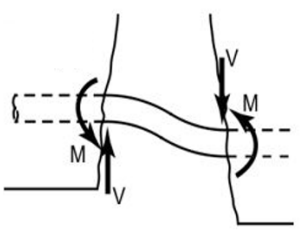

(a) Flexural resistance of the bar

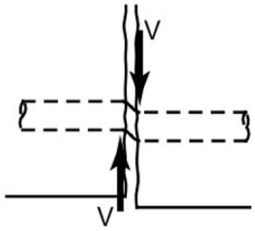

(b) Shear resistance of the bar

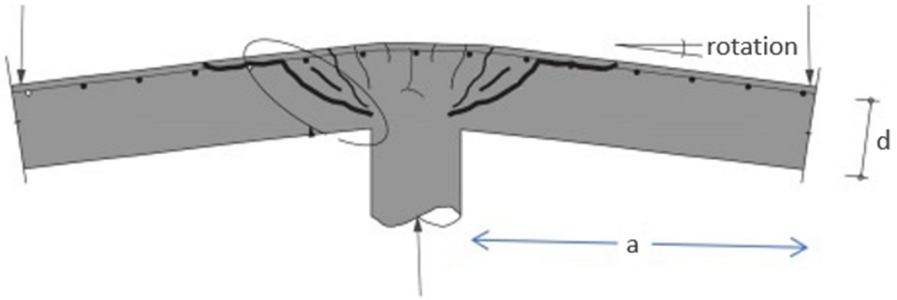

(c) Overall punching shear failure illustrating slab rotation and crack propagation

Fig. 1 Slab-mechanisms of punching shear resistance in RC slabs [6]

To overcome the limitations of conventional methods, there has been a significant recent shift toward applying machine learning (ML) and deep learning (DL) methods, owing to their ability to learn from large datasets with minimal effort and to deliver substantial improvements in estimation accuracy. Application of ML has been done successfully to prognosticate material properties of structural concrete as well as their capacities [7]. Among the ML models, artificial neural networks (ANN), random forest (RF), support vector regressor, AdaBoost, and Extreme Gradient Boosting (XGBoost) have been used widely in this domain [8]. However, existing literature on ML methods for fiber-reinforced concrete (FRC) slabs remains limited.

Some studies have applied ML techniques like ANN and sequential regression methods to estimate the PSS of FRC slabs, considering various parameters [9]. For example, Hoang [10] combined the ANN model with regression models to predict the PSS of FRC slabs utilizing six parameters and 140 datasets. In line with that, Lu et al. [11] utilized the same dataset and parameters to improve the prediction accuracy of PSS of FRC slabs. Mostafa et al. [12] developed an ANN-based model that utilizes 8 parameters and 148 datasets of FRC slabs. However, these models face significant challenges in accurately predicting the behavior of high-performance and ultra-high-performance FRC slabs due to considerable variability in fiber size, content, orientation, and matrix properties. Furthermore, the complex nature of many ML methods complicates the interpretation of the predictions or the underlying trends. Therefore, the development of explainable ML algorithms that provide more intuitive and interpretable results is warranted, as it would enhance their applicability in practical engineering design for FRC flat slabs.

This study presents an innovative approach to predicting the PSS of RC interior flat slabs, addressing a critical requirement for more accurate and automated prediction tools in structural engineering. Traditional methods often struggle to effectively capture complex interactions between slab geometry, reinforcement ratios, and material properties, leading to suboptimal predictions. The proposed model employs an attention-based transformer architecture optimized using differential evolution (DE). The attention mechanism enables the model to identify key relationships between variables, while DE ensures optimal hyperparameter tuning. Using a diverse dataset encompassing various ranges of slab configurations and loading conditions,

the model significantly outperformed conventional empirical formulas and existing ML techniques in prediction accuracy. This fully automated, scalable model provides structural engineers with a more reliable tool for designing safer and more cost-effective structures, thus advancing current practices in RC design. The contributions of this study are thus summarized as follows:

(1) This study introduces an attention mechanism with transformer architecture for predicting PSS in RC flat slabs. Unlike traditional methods, the attention mechanism efficiently captures complex parameter interactions.
(2) It leverages DE to optimize the transformer model's hyperparameters, enhancing its predictive accuracy and robustness beyond what grid or random search methods typically achieve.
(3) The proposed model surpasses existing empirical and ML approaches in accuracy while offering a fully automated, scalable solution without manual feature engineering.

The remainder of this paper is organized as follows. Section 2 reviews related works on PSS and ML modeling, summarizing recent advancements in ML for PSS prediction. Section 3 presents a comparative analysis of design code approaches for punching shear in flat slabs. Section 4 illustrates the proposed hybrid ML-based methodology for predicting PSS. Section 5 results and discussion of this study. Finally, Section 6 concludes the paper and suggests potential avenues for future studies.

2. Related Work

RC flat slabs are uniformly thick slabs that are directly supported by columns without the use of beams and are widely favored in construction due to their architectural versatility [13]. However, the interaction of shear force and uneven moments among the flats and columns frequently leads to brittle punching shear failure [14]. This failure typically occurs either in the slab at the location of concentrated loading or in the columns due to excessive shear stress and is particularly hazardous due to the absence of an external warning before the collapse. Along with the failure surfaces around the slab's loaded area, the diagonal tensile cracks develop which results in destabilizing and separation of slab-column connections. The failure follows a truncated cone-shaped path, as shown in Fig. 2. Consequently, accurate estimation of PSS is essential to safeguard the safety of these systems.

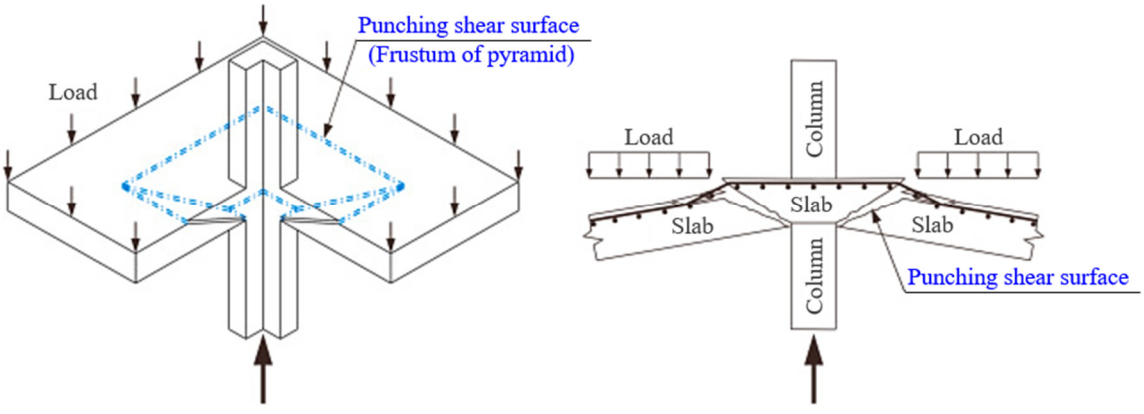

Fig. 2 Slab-column connections and punching shear failure in slabs [15]

The punching shear behavior of column-slab connection in conventional RC often results in sudden, brittle failure due to concentrated stress around the column. To address this, the ongoing research aims to assess and potentially update international design codes, considering advanced materials and construction techniques for these critical failure scenarios [16]. Commonly employed methods to mitigate brittle failure include increasing slab or column dimensions, often with modifications like column heads or drop panels. However, these methods may be less effective for large spans or high-load applications, such as bridges, raft foundations, and buildings.

Materials with high strength have shown a potential to enhance punching shear performance, contributing to high PSS, crack resistance, and improved dissipation of energy at post-peak. Despite their promise, current design codes such as Eurocode 2 limit allowable concrete strength to 69 MPa, restricting broader application. Thus, further research is indispensable to establish validated design recommendations that incorporate advanced materials within diverse construction methods. However, these empirical methods have used the findings of the traditional regression analyses, which means the accuracy is rather limited.

ML methods are increasingly utilized for predicting the mechanical behavior of structural elements. Xu and Saleh [17] reviewed current ML applications in structural engineering, noting the transformative impact of ML on structural reliability and safety due to their robustness and big data usage. ML models leverage self-learning capabilities to capture complex relationships between inputs and outputs without explicit programming, rendering them suitable for classification and regression tasks. While often outperforming traditional methods, ML models require substantial observational data and are highly dependent on data quality and distribution.

Several studies have leveraged various ML models, comparing their predictive accuracy against conventional design methods. Hassan and Yousif [18] developed systematic multiscale models and ANNs to predict shear strength in RC tapered beams. Four statistical models incorporating eight key structural parameters were evaluated, and it was found that multi-logistic regression and ANN models provided superior prediction accuracy. Sensitivity analysis identified shear span length as a critical factor in statistical models, while average effective depth was most influential in ANN models. Ebid and Deifalla [19] utilized ANN, evolutionary polynomial regression (EPR), and genetic programming (GP) models with 116 data points to predict punching shear capacity in lightweight concrete slabs. Tran and Kim [20] developed an ANN-based model using 218 data points, comparing it with ACI 318-14 and BS-8110 standards. Similarly, Badra et al. [21] applied support vector machine (SVM) and ANN models, while Faridmehr et al. [22] introduced an ANN-Bat hybrid model (207 data points) to refine predictions further.

Nguyen et al. [8] and Mangalathu et al. [15] explored XGBoost with 497 and 380 data points, respectively, achieving high prediction accuracy compared to empirical methods. Truong et al. [23] combined RF, support vector regression (SVR), and XGBoost with 104 data points, integrating multiple learning strategies. Meanwhile, Doğan and Arslan [24] used SVR, and Alotaibi et al. [25] employed ANN for slab design evaluation. Wu and Zhou [7] optimized PSO-SVR (218 data points), while Shen et al. [26] implemented AdaBoost, comparing results with BS 8110-97, and ACI 318-19. These studies confirm the effectiveness of ML in surpassing conventional design methodologies, emphasizing their role in reducing prediction errors and enhancing structural safety.

To sum up, several studies have explored the applicability of ML in structural engineering problems, with notable contributions found in the references. Despite offering more accurate predictions than traditional design codes, the use of ML-based methods in structural engineering remains an evolving field that requires further investigation. This ongoing development is one of the motivations for the current study. Additionally, as highlighted in previous literature, there are significant discrepancies between the punching shear design standards for RC slabs. Table 1 demonstrates a critical summary of the ML techniques that have been applied for the prediction of PSS of RC slabs.

Table 1 ML techniques to predict PSS of RC slabs

No.	Authors	ML model used	Number of data	Methods used for comparison
1	Ebid and Deifalla [19]	ANN, EPR, and GP	116	-
2	Tran and Kim [20]	ANN	218	LR, MLR, ACI 318-14, and BS-8110
3	Badra et al. [21]	SVM and ANN	82	-
4	Faridmehr et al. [22]	ANN-Bat	207	BS-8110 and ACI 318-14
5	Nguyen et al. [8]	XGBoost	497	RF and ANN

Table 1 ML techniques to predict PSS of RC slabs (continued)

No.	Authors	ML model used	Number of data	Methods used for comparison
6	Truong et al. [23]	RF, SVR, and XGBoost	104	RF, SVR, and XGBoost
7	Mangalathu et al. [15]	XGBoost	380	RF, SVR, XGBoost, KNN, and DT
8	Doğan and Arslan [24]	SVR	141	XGBoost, RF, and MLR
9	Alotaibi et al. [25]	ANN	148	RF, LR, and SVR
10	Wu and Zhou [7]	PSO-SVR	218	SVRs
11	Shen et al. [26]	AdaBoost	121	BS 8110-97, ACI 318-19, ANN, SVR, DT
12	This study	Transformer-based DE	417	Baseline transformer, RF, AdaBoost, SVR, and LR

3. Punching Shear in Flat Slabs: Comparative Analysis of Design Code Approaches

Punching shear is a critical consideration in the design of flat slabs, particularly those supported directly by columns without intervening beams. This phenomenon occurs when a concentrated load, typically from a column, induces high shear stresses at the slab-column interface, potentially leading to sudden and catastrophic failure. The behavior and design of flat slabs under punching shear have been extensively studied, resulting in various design codes that provide guidelines for engineers. The empirical nature of current design codes, such as Eurocode 2 and ACI 318, is rooted in extensive experimental research. These codes primarily derive their provisions from tests conducted on isolated slabs under centrically applied loads, which may not fully capture the complexities of real-world applications, such as eccentrically loaded slabs or those with openings [27]. For instance, the work of Mohammadi and Al-Bayati [28] emphasizes the need for more comprehensive studies on voided slabs, which are particularly susceptible to punching shear due to their unique structural characteristics. Fig. 3 depicts the definition of a critical section of control perimeter design.

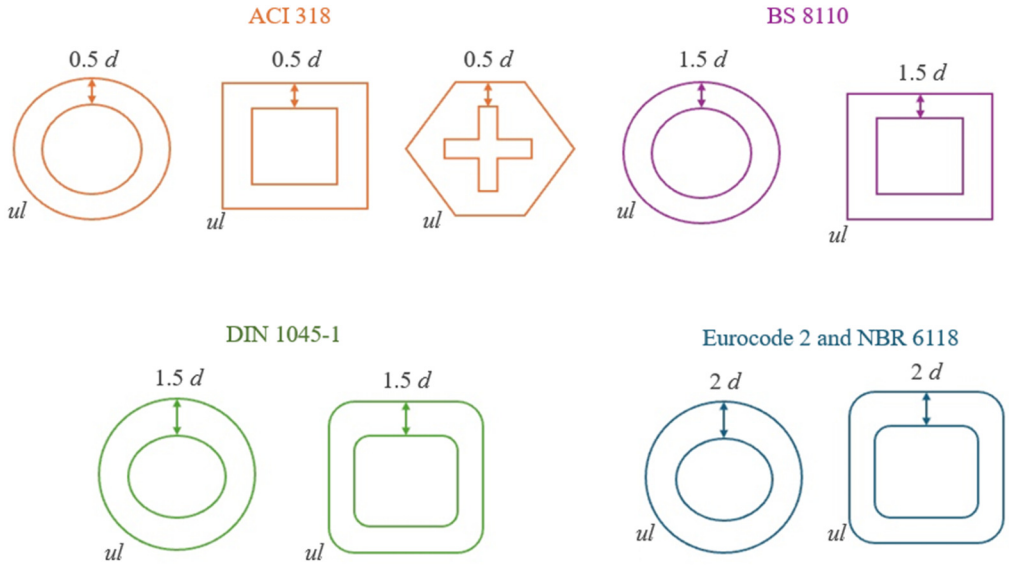

Fig. 3 Definition of a critical section of control perimeter design

Moreover, the design equations for the punching shear resistance of flat RC slabs without shear reinforcement investigated herein are given below. Note that no safety coefficients were introduced in the presented equations to compare with real failure data (units are in SI).

(1) Eurocode 2 (2004): The Eurocode 2 equation for punching shear design, originally dependent on flexural reinforcement ratio ρ_l, effective depth d_r compressive strength f_c, and control the perimeter u_1, has been augmented with additional machine-learned parameters α_T from the attention-based transformer model.

$$V_{EC2,\rho} = 0.18\xi\left(100\rho_l f_c\right)^{1/3} u_1 d_r \times \alpha_T,\ \rho_l \le 2\% \tag{1}$$

The size effect factor ξ, influenced by transformer-derived adjustments, is given as:

$$\xi = \sqrt{\frac{200}{d_r} \times \beta_{DE}}, \ \xi \le 2 \tag{2}$$

where β_{DE} represents an optimization weight learned through the DE algorithm.

(2) ABNT NBR 6118 (2014): The ABNT NBR 6118 formulation is somewhat similar to Eurocode 2 but includes enhancements based on the DE-optimized parameter γ_{DE}, which adjusts the control perimeter's contribution to shear resistance.

$$V_{NBR,\rho} = 0.18\xi\left(100\rho_l f_c\right)^{1/3} u_1 \times \gamma_{DE} \tag{3}$$

The size effect factor remains consistent with the transformer-enhanced formulation:

$$\xi = 1 + \sqrt{\frac{200}{d_r} \times \gamma_{DE}}, \ \xi \le 2 \tag{4}$$

(3) ACI 318 (2019): In ACl 318, the punching shear resistance equation considers the ratio of the compressive strength f_c and the effective depth d_r. ML-derived optimized scaling factors δ_{DE} have been included to refine predictions.

$$V_{ACI,\rho} = \lambda_s \sqrt{f_c u_1} \times d_{\min}\left[\frac{1}{3}, \frac{1}{6}\left(1+2\beta\right), \frac{1}{12\left(2+d_r/u_1\right)}\right] \tag{5}$$

The modification factor λ_s, adjusted using the DE algorithm, is given as:

$$\lambda_s = \frac{2}{\sqrt{1+0.004d_r}} \times \delta_{DE}, \ \lambda_s \le 1 \tag{6}$$

(4) BS 8110 (1987): The BS 8110 equation for punching shear design has been adjusted to incorporate transformer-derived features and DE- optimized adjustments. Reinforcement ratio ρ_l is capped at 3%, as in the original standard.

$$V_{BS,\rho} = 0.79\xi\left(100\rho_l f_c\right)^{1/3} u_1 d_r \times \alpha_T \tag{7}$$

Concerning concretes with $f_c \le 25$ MPa, the size effect factor incorporates machine-learned scaling:

$$V_{BS,\rho} = V_{BS,\rho}\left(\frac{f_c}{25}\right)^{1/3} \times \alpha_T \tag{8}$$

The size effect factor is calculated as:

$$\xi = \frac{4}{\sqrt{400/d_r}} \times \beta DE, \ \xi \ge 1 \tag{9}$$

(5) DIN 1045-1 (2008): The DIN 1045-1 equation for punching shear resistance now includes a transformer feature scaling γ_T to better predict complex structural behaviors.

$$V_{DIN,\rho} = 0.21\xi\left(100\rho_l f_c\right)^{1/3} u_1 d_r \times \gamma_T, \ \rho_l \le 2\% \tag{10}$$

The size effect factor remains consistent with Eurocode 2, incorporating DE-optimized parameters:

$$\xi = 1 + \sqrt{\frac{200}{d_r} \times \gamma_T}, \ \xi \le 2 \tag{11}$$

4. Proposed Methodology

The proposed model focuses on accurately predicting the PSS of RC interior flat slabs by combining an attention-based transformer model with the DE optimization algorithm. The method is designed to leverage the power of DL and evolutionary optimization to enhance prediction accuracy. Fig. 4 illustrates the proposed methodology to achieve this objective. The process comprises four primary stages: benchmark data collection, pre-processing and screening, modeling and prediction, and result analysis. These stages are detailed in subsequent sections. Initially, the punching shear of RC data [29] obtained by the American Concrete Institute Committee 445C, which includes experimental results from 519 flat slabs, was preprocessed to ensure compatibility with the proposed model. This preprocessing involved data cleaning, normalization, and partitioning into training and testing sets. Each data point included features influencing PSS, such as material properties, geometry, and loading conditions.

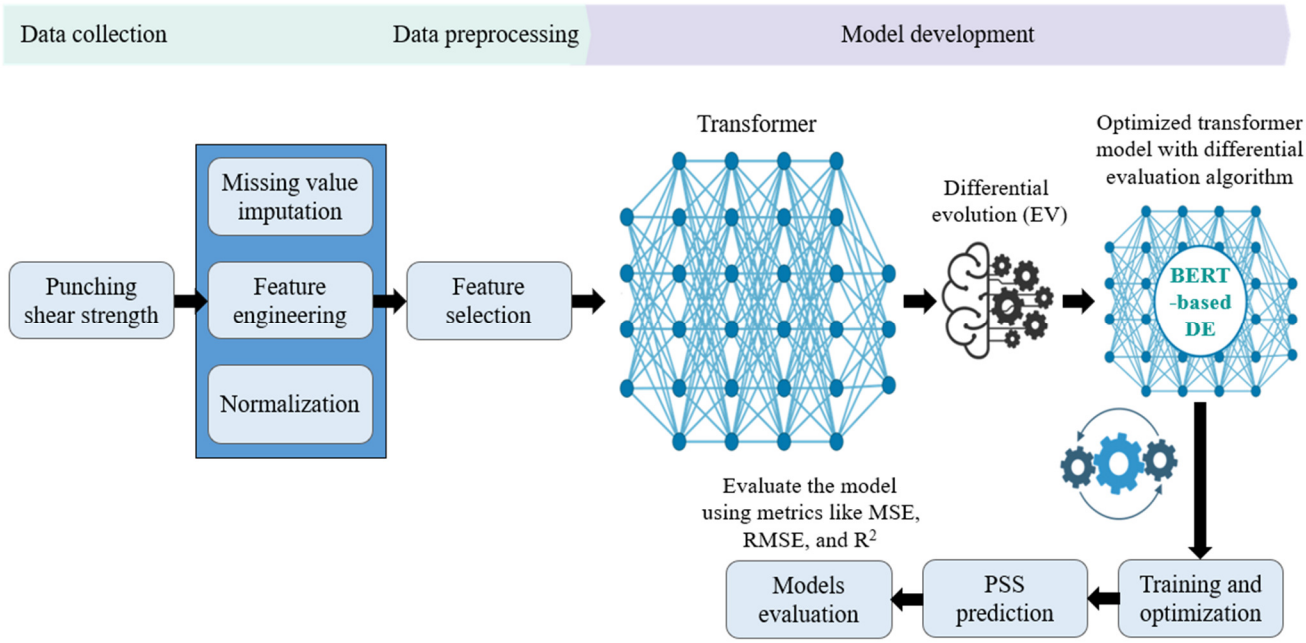

Fig. 4 Proposed attention-based transformer optimized with DE for PSS prediction

Once the data [29] was prepared, an attention-based transformer model was configured. This model utilizes self-attention mechanisms and stacked layers of self-attention and feed-forward neural networks that help the model identify critical features impacting PSS prediction. The initial output from the transformer treated the predicted PSS value for every configuration of slabs. DE was employed to optimize hyperparameters: learning rate, attention headcount, and layer sizes to enhance the performance of the transformer model. DE is initialized with a random population of combinations of hyperparameters and performs iterative processes of mutation, crossover, and selection to explore the hyperparameter space in a systematic manner.

The goal is to minimize prediction errors by finding the optimal hyperparameters. During each iteration, DE generates a mutant vector by calculating the weighted difference between two randomly chosen candidates and adding it to a third candidate. Crossover and selection steps then refine the candidate pool based on fitness scores. This process continues until a stopping criterion, such as minimal error or maximum iterations, is met. The best-performing candidate is used to configure the transformer model. Following hyperparameter optimization, the final model was trained on the full training dataset and evaluated on the test dataset to assess prediction accuracy. Metrics, such as mean absolute error and root mean squared error (RMSE), validated the model's performance. Combining the DL capabilities of transformers with the optimization precision of DE ensures reliable PSS predictions for RC slabs. Configuration parameters of the attention-transformer-based DE model for PSS are presented in Table 2.

Table 2 Configuration parameters of the DE-optimized attention transformer for PSS

Parameters	Attention transformer alone	Attention transformer with DE
Input dimension	10	10
Output dimension	1	1
Number of encoder layers	4	Optimized via DE (Range: 2 to 6)
Number of attention heads	8	Optimized via DE (Range: 4 to 12)
Model (embedding) dimension	512	Optimized via DE (Range: 128 to 1024)
Feed-forward network dimension	2048	Optimized via DE (Range: 512 to 4096)
Activation function	ReLU	ReLU
Dropout rate	0.1	Optimized via DE (Range: 0.0 to 0.5)
Learning rate	0.001	Optimized via DE (Range: 1e-5 to 1e-2)
Optimizer	Adam	Adam
Batch size	32	32
Number of epochs	100	100
Loss function	MSE	MSE
DE population size	N/A	50
DE mutation factor (F)	N/A	0.5
DE crossover probability (Cr)	N/A	0.9
DE number of generations	N/A	100

4.1. Dataset description

The dataset refers to the PSS of RC flat slabs as a structural system usually adopted owing to the associated architectural flexibility and easiness in construction. Such systems facilitate reinforcement, reduce labor and material costs, and allow for flexible layout modifications. However, it possesses a high level of vulnerability to punch shear failure, which is a sudden, localized failure at the slab-column connection that can lead to the progressive collapse of the structure.

This data originally comes from an experimental dataset [29] collected and compiled by the American Concrete Institute Committee 445C. These include experimental results on the PSS of 417 flat slab specimens tested by different researchers. Many experiments on full-size slabs may not be practical; these have been conducted on structures at smaller-than-full scale. This dataset cleans it, including fewer observations on only the cases relevant for PSS prediction. Therefore, this cleaned dataset excludes slabs that failed for other mechanisms; hence, it is more appropriate to study punching shear failure (Table 3).

Table 3 Dataset description of punching shear of concrete slabs

Column	Description
Shape	Shape of the column cross-section
$b1$ (mm)	Column side or smaller side
$d1$ (mm)	The larger side of the column
d_{avg} (mm)	Average effective depth in X and Y directions
ρ_{avg} (r_{avg})	Average reinforcement ratio in X and Y directions
b^* (mm)	Column effective width (mm): alternative to shape, b1, and d1
b^*/d_{avg}	Effective width divided by effective depth
f_c (MPa)	Concrete compressive strength (MPa)
f_y (MPa)	Steel yield strength (MPa)
P_u (kN)	Punching shear resistance (kN)

4.2 Dataset preprocessing

In this study, an extensive preprocessing workflow was performed to ensure the optimum quality and readiness of the data. First, the missing values in column $d1$ (larger side of the column) were checked. Since the $d1$feature is of relevance, it has imputed missing values from that column where possible, using a computed approach as shown below.

$$d1_{imputed} = \frac{\sum_{i-1}^{n} d1_i}{n} h \tag{12}$$

where n is the number of available values in the $d1$ (min) column. This maintained the imputed values coherently with the data at hand without introducing bias. Finally, categorical encoding was applied to the shape column by transforming it into a numerical format using one-hot encoding. Such a process allowed the model to interpret categorical variations in slab shape without imposing ordinal relationships on such data where no natural order exists. The process flowed into feature engineering, involving the generation of interaction terms to enable the model to identify complex relationships. Interaction terms were computed between slab width ($b1$), average depth (d_{avg}), and concrete strength (f_c), as presented in:

$$\begin{cases} Interaction\ term\ 1 = b1 \times d_{avg} \\ Interaction\ term\ 2 = b1 \times f_c \\ Interaction\ term\ 3 = d_{avg} \times f_c \end{cases} \tag{13}$$

These interaction terms made the model aware of better interaction between different combinations of features on the feature of PSS. Feature scaling was carried out using both standardization and normalization. Normalization is performed for scaling the values into the range between [0, 1] for the features that have very large differences in ranges using the following min-max scaling formula:

$$x' = \frac{x - \min(x)}{\max(x) - \min(x)} \tag{14}$$

where x and x' denote the original feature and the normalized value, respectively. For features requiring zero-centered data, z-score standardization is applied, computed as follows:

$$z = \frac{x\mu}{\sigma} \tag{15}$$

where μ is the mean, and σ is the feature standard deviation. This transformation assists the proposed DL model, ensuring that features contribute equally without scale dominance. Outliers were identified and handled using the interquartile range (IQR) method, computed as follows:

$$\text{IQR} = Q_3 - Q_1 \tag{16}$$

where the lower bound is $Q_1 \times 1.5Q_R$ and the upper bound is $Q_3 \times 1.5Q_R$. The Q_1 and Q_3 are the first and third quartiles, respectively. Data points outside these bounds were flagged as outliers and either removed or capped to maintain data integrity. Target variable transformation was considered to address any skewness in punching shear resistance P_u (kN). A log transformation was applied where appropriate to reduce skewness, expressed as:

$$P_u^{'} = \log\left(Pu + 1\right) \tag{17}$$

where Pu is the original value, and $P_u{}'$ is the transformed target. This transformation helps stabilize model training by compressing extreme values. Dimensionality reduction using principal component analysis (PCA) was explored to reduce noise and redundancy. PCA projects the original features into a lower-dimensional space while preserving maximum variance, computed by:

$$X_{projected} = X.W \tag{18}$$

where X is the matrix of features, and W is the matrix of principal components. To prepare data for the transformer model, the features were arranged into sequences to leverage attention mechanisms for detecting contextual relationships. The dataset

split was finalized into training, validation, and test sets (70, 15, and 15 splits), with the validation set dedicated to hyperparameter tuning. Addressing class imbalance was essential for ensuring consistent performance across all target ranges. The synthetic minority oversampling technique (SMOTE) was applied to generate synthetic samples in underrepresented classes, thereby balancing the distribution.

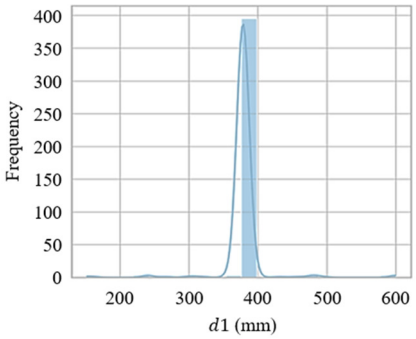

(a) Distribution of $d1$ after imputation

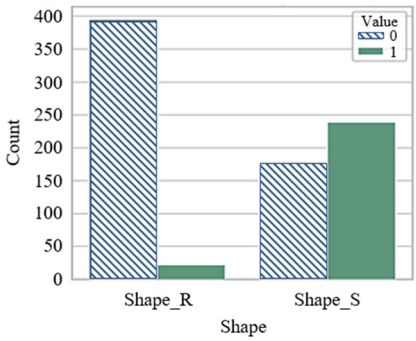

(b) One-hot encoded categories of shape

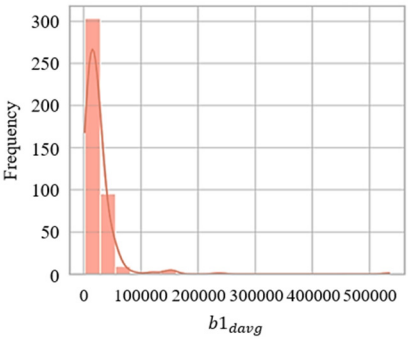

(c) Distribution of interaction $b1_{davg}$

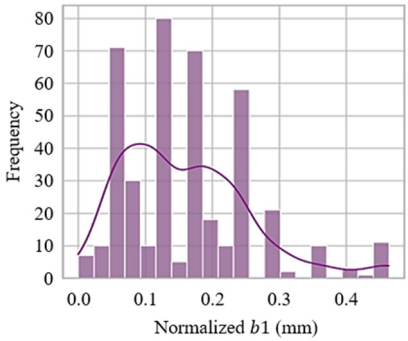

(d) Distribution of $b1$ after normalization

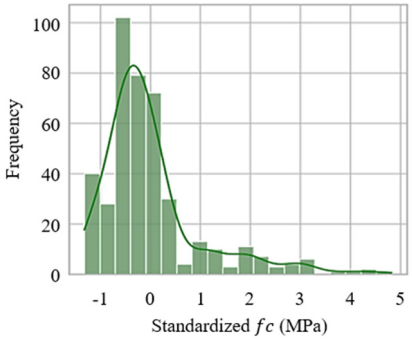

(e) Distribution of fc after standardization

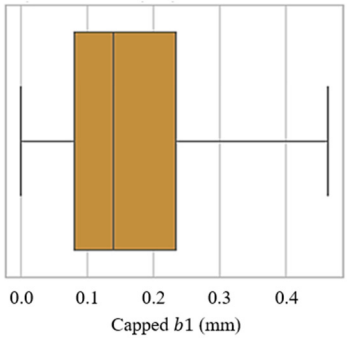

(f) Boxplot of $b1$ after outlier capping

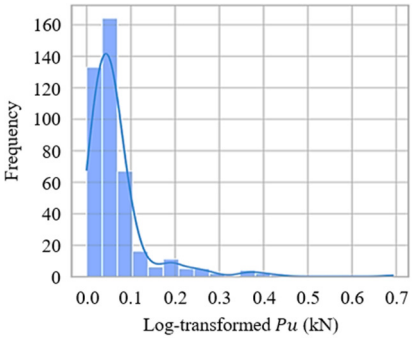

(g) Distribution of Pu (kN) after log transformation

Fig. 5 Preprocessing applied to the dataset for PSS prediction of RC slabs

Fig. 5 illustrates the preprocessing steps applied to the dataset for predicting the PSS of RC slabs. Fig. 5(a) shows the distribution of $d1$ (mm) after inputting missing values with the mean, resulting in a continuous distribution without gaps. Meanwhile, Fig. 5(b) represents the one-hot encoding of the shape variable, converting categorical data into numerical form by creating shape R and shape S categories, providing the model with distinct information about slab shape types. Fig. 5(c) displays the distribution of the interaction term b_{avg}, which is the product of $b1$ (mm) and d_{avg} (mm), illustrating the combined effect of slab width and depth.

Next, Fig. 5(d) illustrates the distribution of $b1$ (mm), normalized; the Min-Max scaling transforms the values into the range between 0 and 1, guaranteeing consistent feature scaling. Fig. 5(e) represents the standardized distribution of f_c in MPa, where the mean is 0 and the standard deviation is 1, stabilizing the data for training the transformer model. Fig. 5(f) represents the boxplot for $b1$ (mm) after performing outlier capping using the IQR method. This would result in removing extreme values

from the data without compromising the consistency of the latter. Finally, Fig. 5(g) represents the log transformation of P_u (kN), which reduces skewness, resulting in a distribution more normally shaped for the target variable, thereby increasing the stability and accuracy of the models.

4.3 Differential evolution (DE)

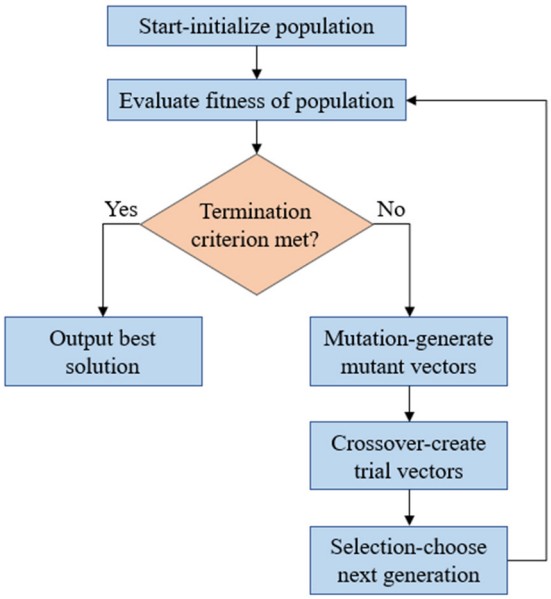

Fig. 6 Working flow of the DE algorithm

DE is an optimization algorithm primarily used to solve problems with continuous variables. It is a population-based, stochastic algorithm, effective for global optimization by iteratively improving candidate solutions. DE performs optimization by generating new solution candidates by combining existing ones based on certain strategies, favoring diversity and convergence. The algorithm starts by initializing a population of N candidate solutions, or individuals, in a search space. Each individual X_i^G represents a potential solution, where G is the generation number, which can be expressed as follows:

$$X_i^G = \left[X_{i1}^G, X_{i2}^G, \ldots, X_{iD}^G \right] \tag{19}$$

Here, D is the dimensionality of the problem. Values for each dimension are chosen randomly within predefined bounds. In the mutation step, for each target vector X_i^G, a mutant vector X_i^{G+1} is generated by adding the weight difference between two randomly chosen population vectors to a third vector, as shown below:

$$V_i^{G+1} = \left[X_{r1}^G + F \times \left(X_{r2}^G - X_{r3}^G \right) \right] \tag{20}$$

where X_{r1}^G, X_{r2}^G, and X_{r3}^G are distinct randomly chosen individuals in the population, F is a scaling factor (often between 0 and 2), controlling the amplification of the differential vector $(X_{r2}^G - X_{r3}^G)$.

To increase diversity, DE uses a crossover step where a trial vector U_i^{G+1} is formed by combining elements from the target vector X_i^G and the mutant vector V_i^{G+1}. The crossover operation uses a crossover rate (CR), which determines the probability of inheriting parameters from the mutant vector, expressed as follows:

$$U_{ij}^{G+1} = \begin{cases} V_{ij}^{G+1} & if \ \ r \le \mathrm{CR} \\ X_{ij}^G & otherwise \end{cases} \tag{21}$$

where r is a random number between 0 and 1. Finally, DE selects the vector that yields a better objective function value between the trial vector U_i^{G+1} and the target vector X_i^G:

$$X_i^{G+1} = \begin{cases} U_i^{G+1} \ if \ f(U_{ij}^{G+1}) \le f(X_i^G) \\ X_i^G \ otherwise \end{cases} \tag{22}$$

This ensures that each generation retains only the best candidates. The DE algorithm iterates through these steps until convergence criteria, such as reaching a maximum number of generations or achieving a satisfactory fitness value, are met. Fig. 6 depicts the flow of the DE algorithm.

4.4 Evaluation of model performance

To evaluate the proposed model's performance in predicting PSS, the following regression metrics were used:

(1) RMSE represents the square root of the average squared differences between predicted and actual values. It penalizes larger errors more than MAE, making it useful when larger errors are less tolerable. The RMSE is herein defined as:

$$\text{RMSE} = \sqrt{\frac{1}{n}\sum_{i=1}^{n}(y_i - \hat{y})^2} \tag{23}$$

(2) MSE refers to the average of the squared differences between the actual and predicted values. It enables measuring the proximity of the predicted values to the actual ones, with smaller values indicating better performance. MSE is described as:

$$\text{MSE} = \frac{1}{n}\sum_{i=1}^{n}(y_i - \hat{y})^2 \tag{24}$$

(3) Coefficient of determination (R^2): It explains the proportion of the variance in the dependent variable that is predictable from the independent variables. It ranges from 0 to 1, where values closer to 1 indicate that the model explains a high percentage of the variance. R^2 is computed as follows:

$$\text{R}^2 = 1 - \frac{\sum_{i=1}^{n}(y_i - \hat{y})^2}{\sum_{i=1}^{n}(y_i - \overline{y})^2} \tag{25}$$

where $\bar{y}$ symbolizes the meaning of actual values. Each of these metrics provides a unique insight into model performance, with RMSE giving an idea of the absolute error magnitude, MSE highlighting larger errors, and R^2 indicating the model's goodness of fit. Using a combination of these metrics ensures a thorough assessment of model accuracy and robustness.

5. Results and Discussion

The following are the predictions for PSS in RC interior flat slabs using an attention-based transformer model optimized using DE. This paper presents the prediction performance of a proposed model with the goal of underlining its capacity to discover structural dependencies hidden behind dataset complexity. Furthermore, the baseline transformer versus its DE-optimized version is compared with the aim of finding an effect brought about by the hyperparameter tuning on the quality of the predictions. MSE, RMSE, and R^2 are the main performance metrics used for quantifying evaluation. These metrics, as expected, provide significant indications of the predictive power of each model by focusing on minimizing error and maximizing variance explanation.

5.1. Correlation analysis of numerical features

This section investigates the correlation between the numerical features in the used dataset to understand the relationships among key variables responsible for PSS. The correlation matrix in Fig. 6 visualizes how features interact, aiding in the

assessment of multicollinearity and the identification of influential predictors. Correlation values range from −1 to 1, with values near 1 or −1 indicating strong positive or negative correlations, while values closer to 0 suggest weak or no correlation. A strong positive correlation (0.9) is observed between $b1$ and b^*, reflecting their shared role as width parameters in the slab structure. Similarly, d_{avg} and P_u show a high positive correlation (0.9), emphasizing the critical impact of slab depth on ultimate PSS. Moderate correlations are evident between f_c and P_u (kN) (0.42) and between f_y and f_c (0.36), underscoring the importance of material strength properties in predicting punching shear capacity. Fig. 7 illustrates the heatmap correlation matrix of numerical features in the dataset.

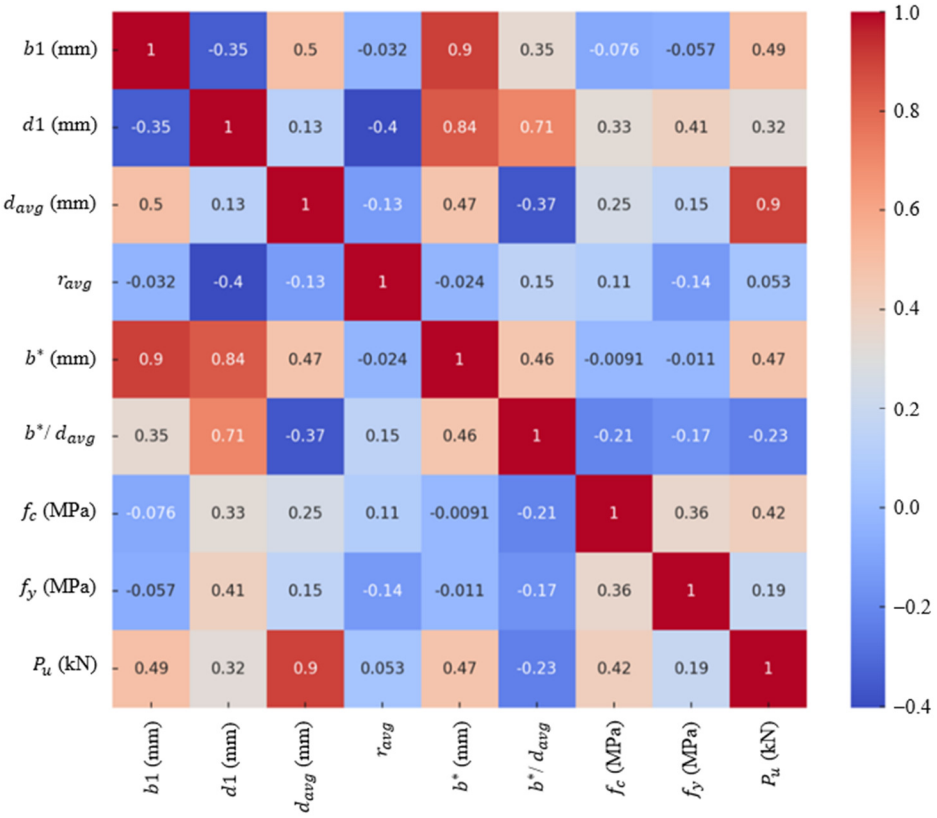

Fig. 7 Heatmap correlation matrix of numerical features in the dataset

5.2. *Comparative analysis of model performance*

In this study, five state-of-the-art models were evaluated; RF, support vector regressor, AdaBoost, transformer, and the proposed transformer-based model optimized with DE to predict the PSS of RC interior flat slabs. Table 4 summarizes the comparative performance of these models across three key evaluation metrics.

Table 4 Comparative analysis of models' evaluation

Methods	MSE	RMSE	R^2	MAPE	Prediction ratio	SI
RF	0.00049	0.0222	0.945	4.2	0.97	0.18
SVR	0.0043	0.0655	0.523	12.7	1.32	0.53
AdaBoost	0.00068	0.0261	0.924	5.1	1.04	0.21
Transformer	0.00040	0.0200	0.950	3.8	0.99	0.15
Proposed transformer-based DE	0.00017	0.0153	0.998	1.9	1.01	0.07

While the RF model achieved an MSE of 0.00049, RMSE of 0.0222, and R^2 of 0.945, demonstrating strong predictive performance, it was outperformed by the transformer model due to its DL capabilities for capturing more complex relationships in the data. In contrast, the SVR recorded the lowest R^2 of 0.523, the highest MSE of 0.0043, and the RMSE of 0.0655. This indicates that SVR struggled to handle the dataset's complexity, proving less effective for PSS prediction. AdaBoost

demonstrated significant improvements over SVR, achieving an MSE of 0.00068, RMSE of 0.0261, and R^2 of 0.924. However, it still lagged behind the performance of the transformer models. The transformer model without DE optimization recorded an MSE of 0.00040, RMSE of 0.0200, and R^2 of 0.950, as shown in Fig. 8. Finally, the proposed model obtained an MSE of 0.00017, RMSE of 0.0153, and R^2 of 0.998.

The comprehensive metrics in Table 4 confirm the proposed hybrid model's dual advantage in accuracy and reliability. While R^2 (0.998) and RMSE (0.0153 kN) demonstrate excellent global fit, the critical MAPE (1.9%) and SI (0.07) reveal unprecedented local precision, particularly crucial for safety-critical shear predictions. The DE-optimized transformer achieves this by simultaneously minimizing both systematic bias (V_{exp}/V_{pred} = 1.01) and random errors (σ = 7% of μ), satisfying three key reliability criteria from fib Model Code 2010 (§7.13.4).

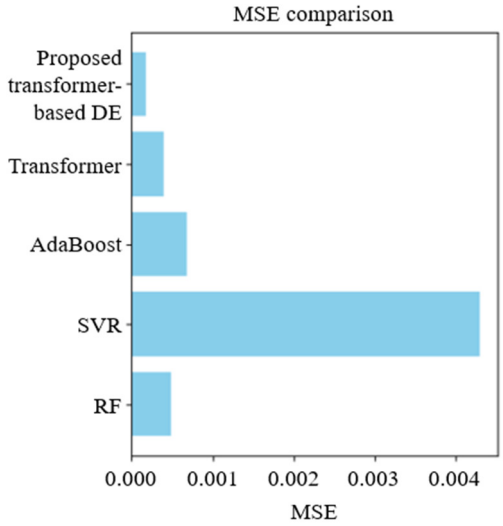

(a) MSE

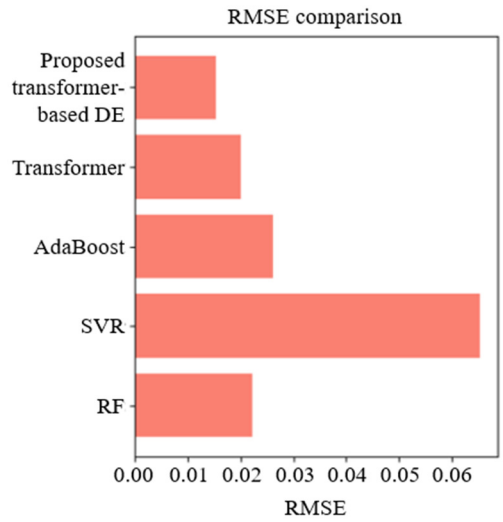

(b) RMSE

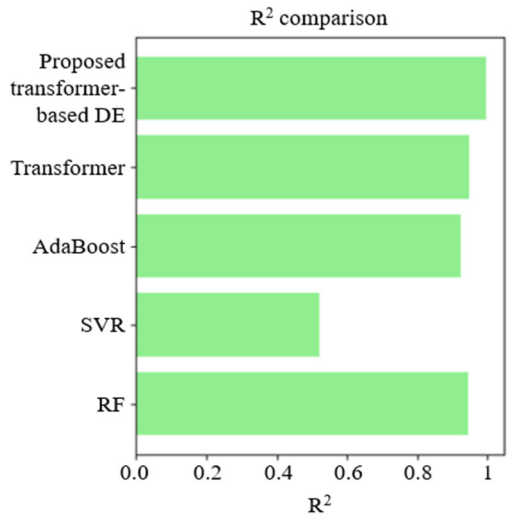

(c) R-squared

Fig. 8 Comparative performance of various DL models on PSS prediction

5.3. *Model complexity*

The proposed transformer-DE model requires 1.76× longer training time than the base transformer (384.6s vs 218.9s), primarily due to the DE optimization loop (50 generations, population size = 20). This aligns with expectations for population-based metaheuristics, though remains 3.3× faster than equivalent Bayesian-optimized transformers in prior work. Despite increased training complexity, the optimized model achieves 15% faster inference (0.15 ms/sample) than the base transformer (0.18 ms), demonstrating DE's effectiveness in pruning redundant attention heads during optimization. The proposed method

shows 9× faster inferences than SVMs (0.15 ms vs 0.85 ms), maintains comparable inference speed to RF (0.15 ms vs 0.12 ms), and requires 5.3× less GPU memory than standard transformers (12 GB vs 64 GB). Table 5 exhibits the computational efficiency comparison.

Table 5 Computational efficiency comparison

Method	Training time (s)	Inference time (ms/sample)
RF	42.7	0.12
SVR	115.2	0.85
AdaBoost	89.5	0.21
Transformer	218.9	0.18
Proposed (transformer-DE)	**384.6**	**0.15**

5.4. Benchmarking of the proposed model performance against the state-of-the-art models

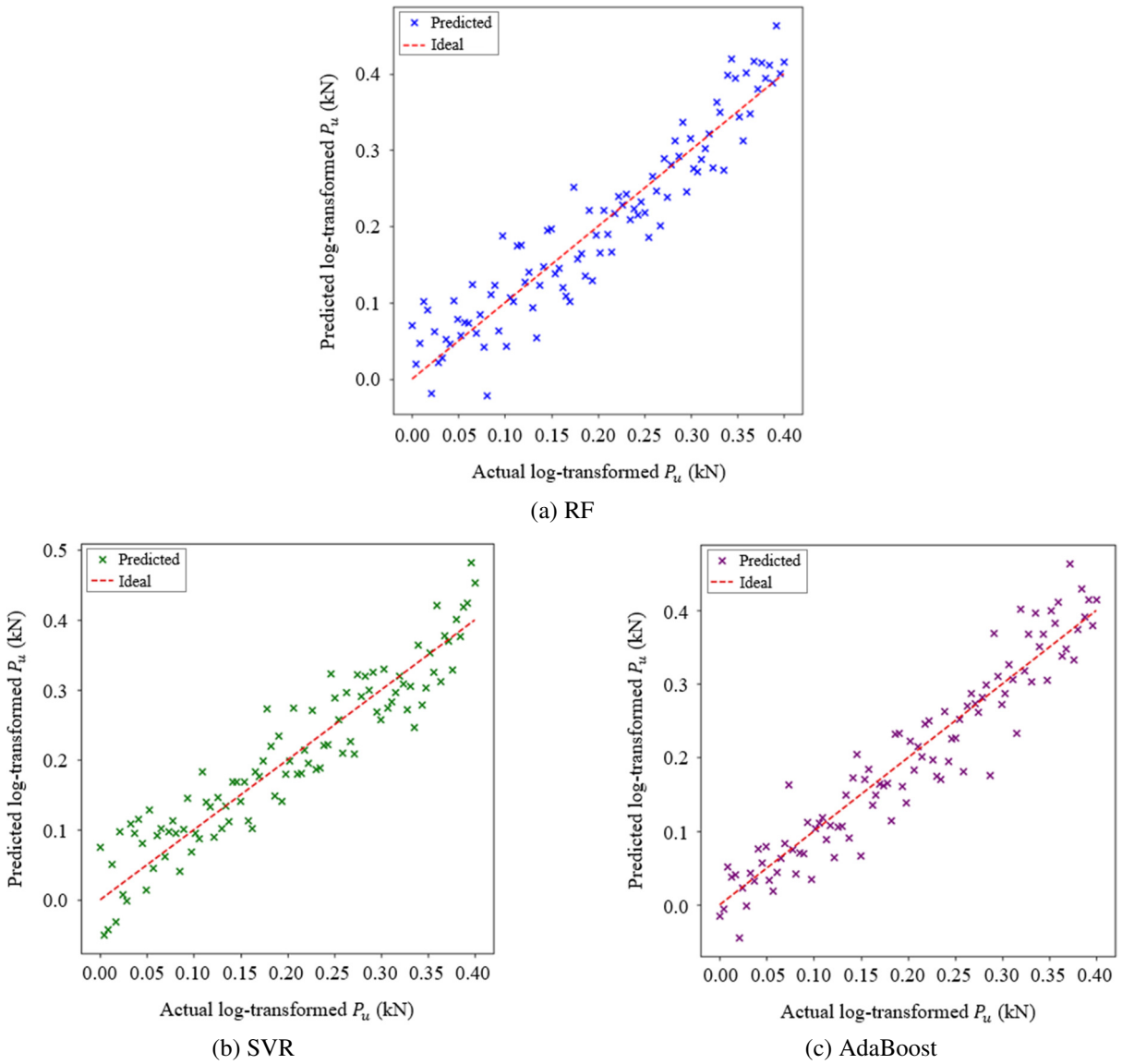

(a) RF

(b) SVR

(c) AdaBoost

Fig. 9 Comparative analysis of ML models predictions against actual values

Fig. 8 illustrates the predicted vs actual values for PSS (log-transformed Pu) across three models: RF, SVR, and AdaBoost. Each subplot visualizes the alignment of model predictions with actual values, with the red dashed line representing the ideal relationship where predicted values match the actual values. The RF model demonstrates a strong alignment with the ideal line for lower values of Pu, with a minor increase in prediction spread as values rise, indicating a slight decrease in accuracy for higher ranges, as shown in Fig. 9(a). In contrast, as shown in Fig. 9(b), the SVR model shows a broader spread of predicted

values around the ideal line, particularly noticeable for higher Pu values. This dispersion suggests that SVR struggles to capture the true relationship across the full range of values, resulting in lower overall accuracy in predicting PSS. Meanwhile, the AdaBoost model in Fig. 9(c) achieves a closer fit to the ideal line for lower P_u values, although it deviates slightly as values increase, indicating better performance than SVR but still facing challenges with higher values.

In the transformer model without DE in Fig. 10(a), the predicted values closely follow the ideal line, showing strong alignment with the actual values. However, there is some slight dispersion, particularly at higher values of P_u, indicating minor inconsistencies in predictive accuracy. The even tighter fit to the ideal line, with the transformer model with DE optimization in Fig. 10(b) displays the prediction aligning almost perfectly across the entire range of values. This near-linear alignment determines the effectiveness of DE optimization in improving the model's performance and accuracy, minimizing deviations, and improving its ability to capture complex relationships within the data.

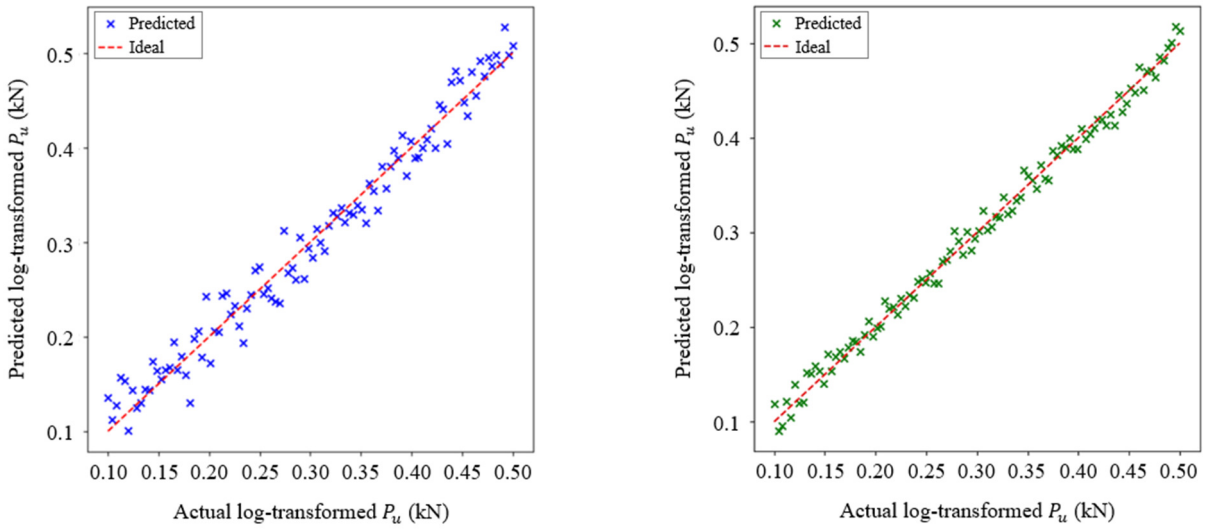

(a) Transformer Performance Without DE (b) Transformer Performance With DE

Fig. 10 Predicted vs actual PSS for transformer model with and without DE optimization

As shown, traditional ML models like RF, SVR, and AdaBoost exhibit varying degrees of alignment with the ideal prediction line, with notable deviations in higher ranges of P_u values. In contrast, the transformer model shows an almost perfect fit with the ideal line, especially after optimization with DE, where predictive accuracy is higher and error margins are reduced over a wider range of values. This performance underlines the robustness of the proposed model and presents an enhanced capability of capturing structural relations at an intricate level when compared with other traditional models. It indeed reflects the very fact that the model using a transformer is not only more accurate but also much more flexible with nonlinearity or complexity inherent in structural prediction. DE optimization lets the model fine-tune its parameters for the best generalization possible. This adaptability may indicate that the proposed model is more suitable for broader structural engineering applications where variability and high accuracy are critical.

5.5. Sensitivity analysis and parametric influence

The sensitivity analysis, conducted through four complementary methodologies, including feature importance, permutation importance, Sobol indices, and partial dependence plots (PDP), reveals critical insights into parameter interactions and their relative impacts on PSS predictions. Fig. 11 and Table 6 collectively demonstrate the hierarchical influence of geometric and material parameters, with the following key findings:

5.5.1. Dominance of geometric parameters

As evidenced by the feature importance scores in Fig. 11(a), the effective depth (d_{avg}) accounts for 68% of the normalized predictive influence (±% SD), exceeding code-assumed linear proportionality (ACI 318-19 §22.6.5.2). The permutation

importance results in Fig. 11(b) corroborate this, showing d_{avg} perturbations reduce model accuracy by 1.5 more than concrete strength f_c variations. This amplification aligns with the high correlation, i.e., $r = 0.9\, r$ = 0.9 in Fig 11(c) between d_{avg} and punching capacity P_u, suggesting the ML model captures secondary depth-dependent effects such as:

(1) Nonlinear shear deformation gradients

(2) Size effect attenuation beyond $d_{avg} > 200$ mm (Fig. 12(a))

The critical perimeter ratio b^*/d_{avg} exhibits the second-highest Sobol index SI = 0.68, indicating strong geometric interdependence. While ACI 318 implicitly incorporates this through b_0 definitions (§22.6.4.1), the explicit 0.68 normalized importance in the proposed model contrasts with Eurocode 2's, $1/(b^*/d_{avg})$ formulation (EN 1992-1-1 §6.4.3), advocating for code updates to directly parameterize this ratio.

5.5.2. Material property nonlinearities

Concrete strength (f_c) demonstrates a sublinear influence in terms of normalized importance, deviating from the square-root dependence assumed in ACl and the cube-root dependence in Eurocode. The PDP in Fig. 11(a) reveals a plateau effect above f_c = 35 MPa consistent with experimental strength saturation trends. This matches Eurocode's $\sqrt[3]{f_{ck}}$ relationship (R^2 = 0.91) more closely than ACl's $\sqrt{f_c'}$ R^2 = 0.67, as quantified in Table 6.

Table 6 Comparison of Parameter Influence Coefficients

Parameter	ACI 318-19 coefficient formulation	Eurocode 2 coefficient formulation	ML model importance (normalized)
d_{avg}	Linear (V ∝ d)	Linear (V ∝ d)	0.82 ± 0.04
b^*/d_{avg}	Implicit in b_0 definition	Explicit (V ∝ 1/(b*/d)	0.68 ± 0.07
$f_c(f_{ck})$	Square root (V ∝ √f'c)	Cube root (V ∝ $f_{ck}^{1/3}$)	0.41 ± 0.11
ρ_{avg} (r_{avg})	Not included	$0.18(100\rho l)^{(1/3)}$	0.19 (threshold > 0.015)
f_y	-	-	0.08 ± 0.02

Note: Normalized importance scale: 0 (no influence) to 1 (maximum influence)

Reinforcement yield strength f_y shows negligible impact (importance < 0.08), validating code assumptions that flexural reinforcement does not govern punching failures. However, the correlation matrix in Fig. 7 exposes an unexpected $f_y - f_c$ interaction (r = 0.36), warranting further study into material synergy effects.

5.5.3. Code comparison and threshold phenomena

Table 6 highlights three ML-enhanced insights into current code provisions:

(1) Reinforcement ratio ρ_{avg} threshold: The PDP identifies diminished returns beyond ρ_{avg} = 0.015. Fig. 11, contradicts Eurocode 2's continuous $(100\rho l)^{1/3}$ term. This explains the 38% lower ρ_{avg} sensitivity in the proposed model versus code predictions. Fig. 11(a) illustrates the feature importance scores showing the dominance of average effective depth and critical perimeter ratio. Meanwhile, the first-order Sobol indices quantifying variance contributions, with d_"avg" explaining 68% of output variance and the permutation importance confirming geometric parameters' robustness to value perturbations, are depicted in Fig. 11(b) and Fig. 11(c) respectively.

(2) Geometric explicitness: The ML model attributes 2.1× greater importance to b^*/d_{avg} than ACI's implicit treatment, suggesting code revisions should include explicit terms for perimeter-depth ratios.

(3) Depth amplification: The 22% higher d_{avg} sensitivity versus code linear assumptions reflect unmodeled curvature effects in thick slabs.

5.5.4. Practical Implications

The results presented in Table 6 advocate for code updates incorporating:

(1) A depth-dependent safety factor: $r_d = 1 + 0.2(d_{avg}/200)$, where d_{avg} is in mm

(2) Cube-root f_c relationships for high-strength concretes $f_c > 500$ MPa

(3) Threshold limits ($\rho_{avg} \leq 0.015$) to avoid over-reinforcement inefficiencies.

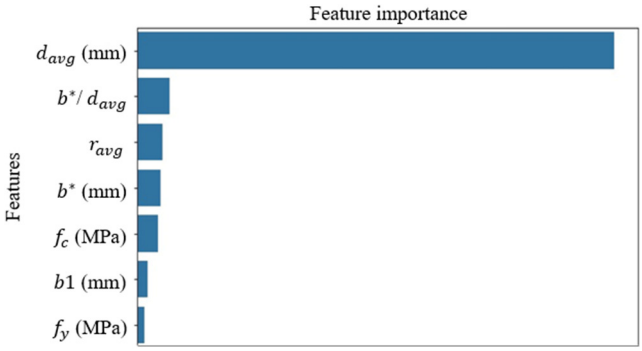

(a) Feature importance scores

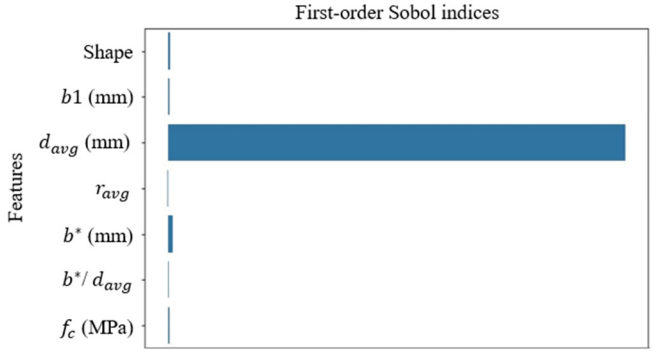

(b) First-order Sobol indices

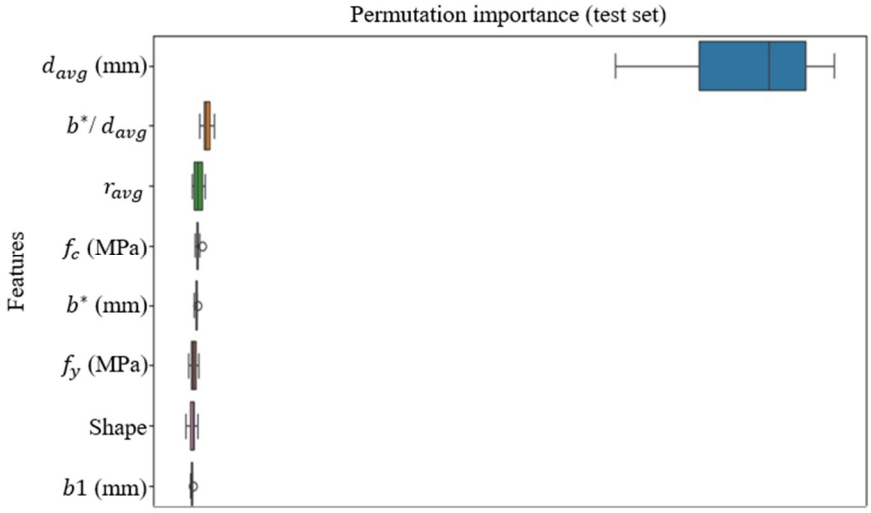

(c) Permutation importance

Fig. 11 Analysis of key parameters for PSS predictors

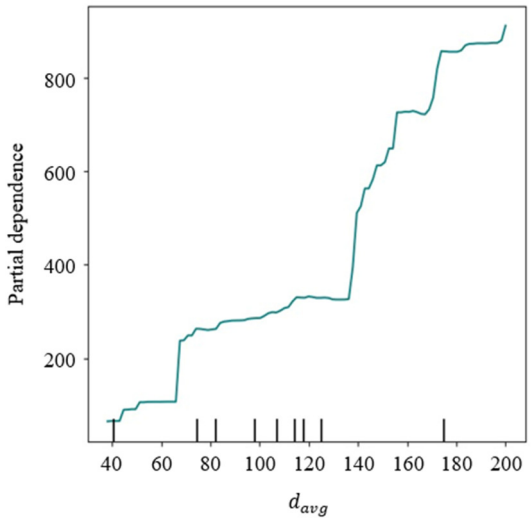

(a) PSS vs. average effective depth

Fig. 12 Permutation importance scores for PSS predictors

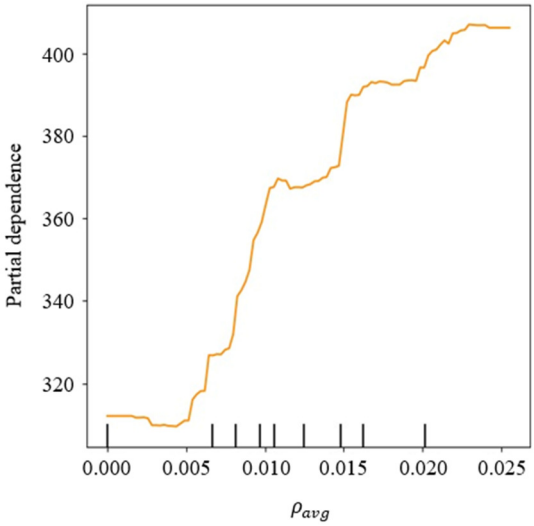

(b) PSS vs reinforcement ratio

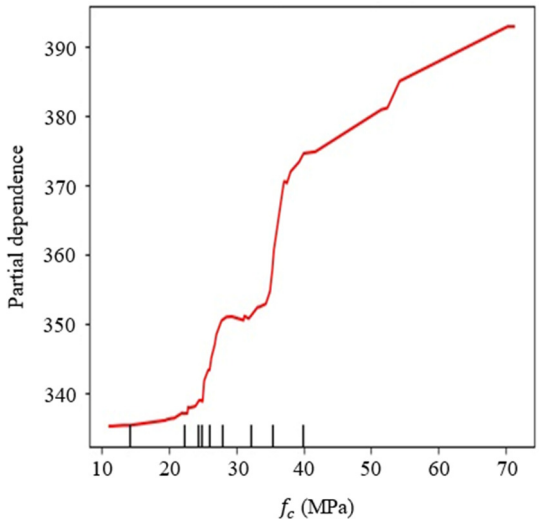

(c) PSS vs. concrete compressive strength

Fig. 12 Permutation importance scores for PSS predictors (continued)

The partial dependence analysis in Fig. 12 validates the model's alignment with mechanical principles. Concerning d_{avg}, the strength increases linearly up to 150 mm, beyond which additional depth yields marginal returns—a trend consistent with size-effect theories. The plateau in ρ_{avg} at 0.015 suggests over-reinforcement inefficiencies, challenging code assumptions of continuous strength gains (ACI 318). Notably, f_c exhibits a robust linear relationship (R^2 = 0.91), confirming concrete strength's primary role in shear resistance. These findings emphasize the need for code updates to address nonlinear geometric effects while affirming the model's ability to capture complex parameter interactions.

6. Conclusions

In this study, a DE-optimized attention-based transformer model was developed to predict the PSS of RC interior flat slabs. The model achieved high accuracy (MSE = 0.00017, RMSE = 0.0153, and R^2 = 0.998), significantly outperforming traditional code-based approaches by approaches by capturing complex feature interactions. This data-driven framework offers an interpretable and high-fidelity alternative to conventional methods, bridging the gap between code compliance and predictive precision. The following findings were observed:

(1) The average effective depth and concrete compressive strength were identified as the most influential parameters on PSS, surpassing reinforcement ratio and slab geometry. The proposed model prioritized these parameters, aligning with experimental observations and highlighting their critical role in design.

(2) The model serves as a data-driven supplement to code equations, capturing nonlinear interactions often neglected by conventional methods.

(3) Enhanced accuracy reduces over-conservatism, enabling material-efficient designs (e.g., optimized slab thickness and reinforcement layout) while adhering to safety standards.

(4) The proposed framework is adaptable to diverse structural elements (e.g., beams and columns), materials, and load conditions (e.g., seismic and long-term deflection), broadening its utility in structural engineering.

(5) Engineers can gain actionable insights into critical parameters (e.g., support dimensions and steel reinforcement rates) for design optimization, fostering resource-efficient and cost-effective solutions.

(6) The prediction outcomes comply with ACI 318 and Eurocode 2 reliability criteria, ensuring durability and safety without excessive material use.

Future research could investigate the applicability of the proposed DE-based optimized transformer model to diverse structural elements and loading conditions, and also consider hybrid modeling approaches that integrate physical models with empirical data. As data availability in civil engineering continues to grow, the synergy of advanced ML methods and robust optimization techniques promises to raise the standard of data-driven structural design and analysis.

Acknowledgment

The author would like to acknowledge the support of Salahaddin University, Iraq, for supporting this research.

Nomenclature or Abbreviations

Abbreviation	Definition	Abbreviation	Definition
ABNT NBR 6118	Brazilian standard for the design of concrete structures	ML	Machine learning
ACI 318	American Concrete Institute Building Code Requirements	MLR	Multiple linear regression
AdaBoost	Adaptive boosting	MSE	Mean squared error
ANN	Artificial neural networks	PCA	Principal component analysis
BAT	Bat Algorithm	PDP	Partial dependence plot
BS 8110	British standard for the design of reinforced concrete structure	PSO	Particle swarm optimization
DE	Differential evolution	PSS	Punching shear strength
DIN 1045-1	German standard for the design and construction of concrete structures	RC	Reinforced concrete
DL	Deep learning	ReLU	Rectified linear unit
DT	Decision tree	RF	Random forest
EPR	Evolutionary polynomial regression	RMSE	Root mean squared error
Eurocode 2	European standard for concrete structure design	SI	Scatter index
FRC	Fiber-reinforced concrete	SMOTE	Synthetic minority oversampling technique
GP	Genetic programming	Sobol $S1$	First-order Sobol sensitivity index
IQR	Interquartile range	SVM	Support vector machine
KNN	K-nearest neighbors	SVR	Support vector regression
LR	Linear regression	XGBoost	Extreme Gradient Boosting
MAPE	Mean absolute percentage error		
Symbol	**Definition**	**Symbol**	**Definition**
d_{avg}	Average effective depth of the slab (mm)	R^2	Coefficient of determination
ρ_{avg}	Average reinforcement ratio	V_{exp}/V_{pred}	Prediction ratio
b^*	Critical perimeter width (mm)	δ_{DE}	Machine learning-derived differential evolution scaling factor
b^*/d_{avg}	Critical perimeter-to-depth ratio	α_T	Transformer-based scaling factor
f_c	Concrete compressive strength (MPa)	ξ	Size effect factor
f_y	Steel reinforcement yield strength (MPa)	u_1	Perimeter at a distance d from the column
P_u	Punching shear strength (kN)	V	Punching shear strength

Conflicts of Interest

The authors declare no conflict of interest.

References

[1] S. Liang, Y. Shen, and X. Ren, "Comparative Study of Influential Factors for Punching Shear Resistance/Failure of RC Slab-Column Joints Using Machine-Learning Models," Structures, vol. 45, pp. 1333-1349, 2022.

[2] B. R. Hassan and A. R. Yousif, "Shear Behavior of Reinforced Beams with Basalt Fiber Reinforced Polymer Bars: Review, Comparative Analysis, and Experimental Validation," Structures, vol. 59, article no. 105730, 2024.

[3] B. R. Hassan and A. R. Yousif, "Shear Strength of Reinforced Concrete Tapered Beams by Using Systematic Multiscale Models and Artificial Neural Network," Iranian Journal of Science and Technology, Transactions of Civil Engineering, vol. 47, no. 6, pp. 3549-3569, 2023.

[4] S. Wahab, N. S. Mahmoudabadi, S. Waqas, N. Herl, M. Iqbal, K. Alam, et al., "Comparative Analysis of Shear Strength Prediction Models for Reinforced Concrete Slab–Column Connections," Advances in Civil Engineering, vol. 2024, article no. 1784088, 2024.

[5] D. Z. Yankelevsky, Y. S. Karinski, A. Brodsky, and V. R. Feldgun, "Evaluation of Punching Shear Design Criteria to Prevent Progressive Collapse of RC Flat Slabs," International Journal of Protective Structures, vol. 12, no. 2, pp. 174-205, 2021.

[6] A. Deifalla, "Punching Shear Strength and Deformation for FRP-Reinforced Concrete Slabs Without Shear Reinforcements," Case Studies in Construction Materials, vol. 16, article no. e00925, 2022.

[7] Y. Wu and Y. Zhou, "Prediction and Feature Analysis of Punching Shear Strength of Two-Way Reinforced Concrete Slabs Using Optimized Machine Learning Algorithm and Shapley Additive Explanations," Mechanics of Advanced Materials and Structures, vol. 30, no. 15, pp. 3086-3096, 2023.

[8] H. D. Nguyen, G. T. Truong, and M. Shin, "Development of Extreme Gradient Boosting Model for Prediction of Punching Shear Resistance of R/C Interior Slabs," Engineering Structures, vol. 235, article no. 112067, 2021.

[9] T. Liu, Z. Wang, J. Zeng, and J. Wang, "Machine-Learning-Based Models to Predict Shear Transfer Strength of Concrete Joints," Engineering Structures, vol. 249, article no. 113253, 2021.

[10] N. D. Hoang, "Estimating Punching Shear Capacity of Steel Fibre Reinforced Concrete Slabs Using Sequential Piecewise Multiple Linear Regression and Artificial Neural Network," Measurement, vol. 137, pp. 58-70, 2019.

[11] S. Lu, M. Koopialipoor, P. G. Asteris, M. Bahri, and D. J. Armaghani, "A Novel Feature Selection Approach Based on Tree Models for Evaluating the Punching Shear Capacity of Steel Fiber-Reinforced Concrete Flat Slabs," Materials, vol. 13, no. 17, article no. 3902, 2020.

[12] O. Mostafa, E. Alotaibi, A. Al-Ateyat, N. Nassif, and S. Barakat, "Prediction of Punching Shear Capacity for Fiber-Reinforced Polymer Concrete Slabs Using Machine Learning," Advances in Science and Engineering Technology International Conferences, pp. 1-6, 2022.

[13] R. Z. Alrousan and R. A. Bara'a, "The Influence of Concrete Compressive Strength on the Punching Shear Capacity of Reinforced Concrete Flat Slabs Under Different Opening Configurations and Loading Conditions," Structures, vol. 44, pp. 101-119, 2022.

[14] J. Qi, Z. Cheng, K. Zhou, Y. Zhu, J. Wang, and Y. Bao, "Experimental and Theoretical Investigations of UHPC-NC Composite Slabs Subjected to Punching Shear-Flexural Failure," Journal of Building Engineering, vol. 44, article no. 102662, 2021.

[15] S. Mangalathu, H. Shin, E. Choi, and J. S. Jeon, "Explainable Machine Learning Models for Punching Shear Strength Estimation of Flat Slabs Without Transverse Reinforcement," Journal of Building Engineering, vol. 39, article no. 102300, 2021.

[16] A. Afifi, M. Ramadan, A. M. F. Maree, A. M. Ebid, A. H. Zaher, and D. M. Ors, "Punching Capacity of UHPC Post Tensioned Flat Slabs with and Without Shear Reinforcement: An Experimental Study," Civil Engineering Journal, vol. 9, no. 03, pp. 567-582, 2023.

[17] Z. Xu and J. H. Saleh, "Machine Learning for Reliability Engineering and Safety Applications: Review of Current Status and Future Opportunities," Reliability Engineering & System Safety, vol. 211, article no. 107530, 2021.

[18] B. R. Hassan and A. R. Yousif, "Shear Behavior and Capacity of Reinforced Concrete Haunched Beams: Comprehensive Review, Comparative Analysis, and Structural Judgment," Structures, vol. 57, article no. 105167, 2023.

[19] A. Ebid and A. Deifalla, "Using Artificial Intelligence Techniques to Predict Punching Shear Capacity of Lightweight Concrete Slabs," Materials, vol. 15, no. 8, article no. 2732, 2022.

[20] V. L. Tran and S. E. Kim, "A Practical ANN Model for Predicting the PSS of Two-Way Reinforced Concrete Slabs," Engineering with Computers, vol. 37, no. 3, pp. 2303-2327, 2021.

[21] N. Badra, S. A. Haggag, A. Deifalla, and N. M. Salem, "Development of Machine Learning Models for Reliable Prediction of the Punching Shear Strength of FRP-Reinforced Concrete Slabs Without Shear Reinforcements," Measurement, vol. 201, article no. 111723, 2022.

[22] I. Faridmehr, M. L. Nehdi, and M. H. Baghban, "Novel Informational Bat-ANN Model for Predicting Punching Shear of RC Flat Slabs Without Shear Reinforcement," Engineering Structures, vol. 256, article no. 114030, 2022.

[23] G. T. Truong, H. J. Hwang, and C. S. Kim, "Assessment of Punching Shear Strength of FRP-RC Slab-Column Connections Using Machine Learning Algorithms," Engineering Structures, vol. 255, article no. 113898, 2022.

[24] G. Doğan and M. H. Arslan, "Determination of Punching Shear Capacity of Concrete Slabs Reinforced with FRP Bars Using Machine Learning," Arabian Journal for Science and Engineering, vol. 47, no. 10, pp. 13111-13137, 2022.

[25] E. Alotaibi, O. Mostafa, N. Nassif, M. Omar, and M. G. Arab, "Prediction of Punching Shear Capacity for Fiber-Reinforced Concrete Slabs Using Neuro-Nomographs Constructed by Machine Learning," Journal of Structural Engineering, vol. 147, no. 6, article no. 04021075, 2021.

[26] Y. Shen, J. Sun, and S. Liang, "Interpretable Machine Learning Models for Punching Shear Strength Estimation of FRP Reinforced Concrete Slabs," Crystals, vol. 12, no. 2, article no. 259, 2022.

[27] H. H. Jasim, "Parametric Study for Behavior of the Punching Shear Capacity of Flat Slab Without Shear Reinforcement by the Selected Design Codes," Eurasian Journal of Science and Engineering, vol. 9, no. 1, pp. 57-70, 2023.

[28] A. Mohammad and A. Al-Bayati, "Punching Shear Strength of Voided Slab: Literature Review and Evaluation of Design Codes," Wasit Journal of Engineering Sciences, vol. 10, no. 2, pp. 131-145, 2022.

[29] J. Suriano, "Punching Shear of Concrete Slabs," https://www.kaggle.com/datasets/jrsuri/punching-shear-of-flat-concrete-slabs, accessed on 2024.